Inorganic Chemistry

pubs.acs.org/IC

Article

Thiosemicarbazone Derivatives as Inhibitors of Amyloid-β Aggregation: Effect of Metal Coordination

Ana I. Matesanz, Ana B. Caballero, Carmen Lorenzo, Alba Espargaró, Raimon Sabaté, Adoración G. Quiroga,* and Patrick Gamez*

Cite This: https://dx.doi.org/10.1021/acs.inorgchem.0c00467

Read Online

ACCESS | Metrics & More | Article Recommendations | Supporting Information

ABSTRACT: Three thiosemicarbazone derivatives, namely 4-(dimethylamino)-benzaldehyde 4,4-dimethylthiosemicarbazone (HL^1), 4-(dimethylamino)-benzaldehyde thiosemicarbazone (HL^2), and 4-(dimethylamino)benzaldehyde 4-methylthiosemicarbazone (HL^3), have been synthesized and characterized. The three palladium(II) complexes **1**−**3** were prepared respectively from HL^1, HL^2, and HL^3. The crystal structures of two coordination compounds, namely $Pd(L^2)_2$ (**2**) and $Pd(L^3)_2$ (**3**), were obtained, which showed the expected square-planar environment for the metal centers. The ligand HL^3 and the Pd(II) complexes **1**−**3**, which are stable in buffered solutions containing up to 5% DMSO, exhibit remarkable inhibitory properties against the aggregation of amyloid-β, reducing the formation of fibrils. HL^1, HL^3, **2**, and **3** display IC_{50} values (i.e., the concentrations required to reduce Aβ fibrillation by 50%) below 1 μM, lower that of the reference compound catechin (IC_{50} = 2.8 μM). Finally, *in cellulo* studies with *E. coli* cells revealed that the palladium(II) compounds are significantly more efficient than the free ligands in inhibiting Aβ aggregation inside bacterial inclusion bodies, thus illustrating a beneficial effect of metal coordination.

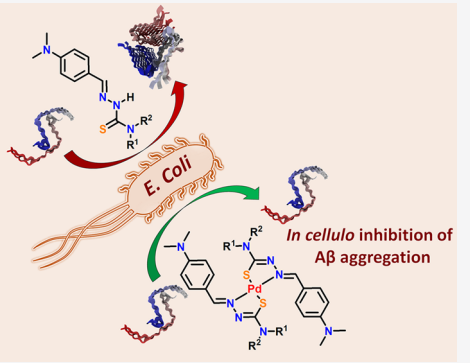

INTRODUCTION

Alzheimer's disease (AD) is a neurodegenerative disorder characterized by the progressive loss of cholinergic neurons, resulting in cognitive decline.[1] AD is the leading cause of dementia, currently affecting about 50 million people worldwide.[2] To date, there are no efficient treatments against the disease or effective tools to diagnose it at its very early stage.[3] Therefore, the development of new diagnostic and therapeutic strategies is of paramount importance, as the number of AD patients is rapidly increasing, which also causes a large economic burden on society.[4]

The extracellular aggregation of amyloid-β (Aβ) observed in AD brains represents one of the hallmarks of the disease.[5,6] This accumulation of amorphous Aβ deposits produces senile plaques, which contain high amounts of Cu and Fe.[7,8] It has been demonstrated that these redox-active metal ions facilitate Aβ aggregation[8,9] and mediate the generation of reactive oxygen species (ROS).[10] Therefore, the development of molecules that may control/avoid the abnormal accumulation of Aβ in the brain (i.e., amyloid cascade) may act as efficient agents to treat AD.

Thiosemicarbazones (TSCNs) and their metal complexes have been used in many pharmaceutical applications:[11,12] for instance, as antiparasital,[13] antibacterial,[14] antiretroviral,[15] and anticancer agents.[16−18] Triapine is a well-known thiosemicarbazone derivative, which has undergone clinical trials as a potential chemotherapeutic drug, together with some of its analogues.[16,19−21] It can be stressed here that the potential of TSCNs toward the inhibition of Aβ aggregation has not been extensively explored; some recent studies have highlighted interesting neuroprotective properties of a variety of thiosemicarbazone compounds.[22−25] Some metal TSCN complexes have been reported as well for their antiaggregation properties; for instance, some Ru(II) complexes bearing indole thiosemicarbazones showed inhibitory potential against the aggregation of Aβ(1−42).[26] Copper and zinc thiosemicarbazone complexes have also been described to reduce the levels of Aβ, *in vitro*.[27]

The antiaggregation properties of TSCN-based molecules have been associated with their planarity, especially if they contain aromatic substituents.[23,28] The presence of planar aromatic moieties in the inhibitors of aggregation appears to be important for their hydrophobic interactions with Aβ: for instance, through π-stacking contacts.[29] Recently, a series of arene-containing TSCNs (namely with a naphthyl, anthracenyl, or pyrenyl group) have been reported whose antiaggregation efficiencies, analyzed by docking studies, were ascribed to

Received: February 14, 2020

their ability to interact hydrophobically with the aggregation-prone stretch of the peptide; in particular, strong π interactions were observed with particular amino acid residues, viz. Ser 26, Asn 27, Phe 20, Leu 17, and Lys 16, together with hydrogen bonds.[22]

Considering the highly promising results reported for thiosemicarbazones in the area of anti-AD drug design (see above),[30,31] we have decided to design and prepare three new 4-(dimethylamino)benzaldehyde thiosemicarbazone derivatives, viz. **HL**^{1}, **HL**^{2}, and **HL**^{3} (Scheme 1), comprising the same aryl ring and distinct hydrogen-bonding capabilities (provided by the terminal amine group; see **R**^{1} and **R**^{2} groups in Scheme 1).

Scheme 1. Structures of the Thiosemicarbazone Ligands and Synthetic Pathway to Their Corresponding Palladium(II) Complexes

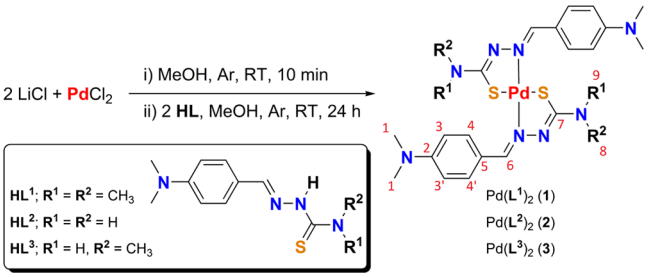

We subsequently prepared the corresponding palladium(II) complexes, viz. Pd(**L**^{1})$_2$ (**1**) Pd(**L**^{2})$_2$ (**2**), and Pd(**L**^{3})$_2$ (**3**) (Scheme 1), with the objective to investigate and compare their antiaggregation properties with those of the free ligands. Palladium(II) was purposely chosen for the square-planar geometry typically obtained upon coordination and was preferred to platinum(II) due to the better solubility of palladium complexes.[32,33] The aim was to rigidify the systems through metal binding and generate planar and extended structures. Indeed, free TSCNs exhibit a certain degree of rotational freedom, which is illustrated in Chart 1 with 4-nitrobenzaldehyde thiosemicarbazone (**TSCN-H**), whose crystal structure has been reported.[34] While rotation is possible around the N−N bond for the free ligand, the system becomes rigid upon coordination with palladium (**TSCN-Pd**); furthermore, the ligand changes its conformation from *trans-trans* to *cis-cis* (see bonds in blue in Chart 1), as revealed by its reported crystal structure.[34]

In vitro aggregation studies with Aβ(1−40) revealed disparities between the free TSCN ligands **HL**^{1}−**HL**^{3} and the corresponding palladium(II) complexes **1**−**3**, with IC$_{50}$ values (viz. the concentrations required to decrease Aβ aggregation by 50%) in the nanomolar to low micromolar range. Even more interestingly, *in cellulo* studies with *Escherichia coli* cells expressing Aβ(1−42) in inclusion bodies[35] showed drastically distinct behaviors between the free organic molecules and the metal-containing compounds, the latter being significantly more efficient.

RESULTS AND DISCUSSION

Synthesis and Characterization of the Compounds. The thiosemicarbazone ligands **HL**^{1}, **HL**^{2}, and **HL**^{3} were prepared applying a known synthetic procedure,[36] consisting of a condensation reaction between 4-(dimethylamino)-benzaldehyde and the corresponding thiosemicarbazide derivative (see Experimental Section for details).

The palladium complexes Pd(**L**^{1})$_2$ (**1**), Pd(**L**^{2})$_2$ (**2**), and Pd(**L**^{3})$_2$ (**3**) were prepared through the reaction of a methanolic solution of Li_2PdCl_4 (generated *in situ*) with 2 equiv of the corresponding ligand (**HL**^{1}, **HL**^{2}, or **HL**^{3}) suspended in methanol (see Scheme 1 and the Experimental Section for details).

All compounds were fully characterized by analytical and spectroscopic techniques. The ^{1}H NMR spectra of complexes **1**−**3** showed similar profile, the AA′BB′ system for the phenyl groups of the ligands being maintained upon coordination to the metal center; the signals for the hydrogens H7 and H4/4′ are the most affected due to their proximity to the palladium atom. The ^{13}C NMR chemical shifts corresponding to the C atoms adjacent to the N-donor atom move to lower values. Analytical data including those of mass spectrometry agree with the general formula proposed: i.e., Pd(L)$_2$ (Scheme 1). Moreover, single crystals of **2** and **3** were obtained and their X-ray structures were determined, which are depicted in Figure 1.

Crystallographic and refinement parameters for **2** and **3** are summarized in Table S1. Selected bond distances and angles for **2** and **3** are given in Tables S2 and S3, respectively. The solid-state structures of the two compounds are flat, as anticipated; for both of them, the metal center is in a slightly distorted square-planar environment formed by two sulfur atoms (monoanionic form of the ligand) and two nitrogen atoms belonging to two different ligands, which are *trans* to each other. The metal−chelate rings and the dimethylamino arenes are coplanar. It can be pointed out that **2** is isostructural with its previously reported nickel analogue.[37] While the crystal lattice of **3** does not contain any solvent molecules, that of **2** includes two molecules of DMSO (Figure 1), which are hydrogen-bonded (through their oxygen atom) to the nitrogen atom N3 of the two ligands (N3−H···O = 2.903(9) Å). The crystal packing of Pd(**L**^{3})$_2$ (**3**) reveals the occurrence of π−π

Chart 1. Structure of Free 4-Nitrobenzaldehyde Thiosemicarbazone (TSCN-H) and of Its Palladium(II) Complex[34] [a]

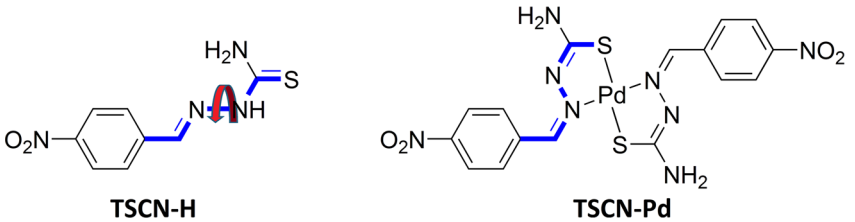

[a]The red arrow illustrates the N−N rotation for the free ligand, and the bonds in blue show the change in conformation from the free to the coordinated ligand.

https://dx.doi.org/10.1021/acs.inorgchem.0c00467
Inorg. Chem. XXXX, XXX, XXX−XXX

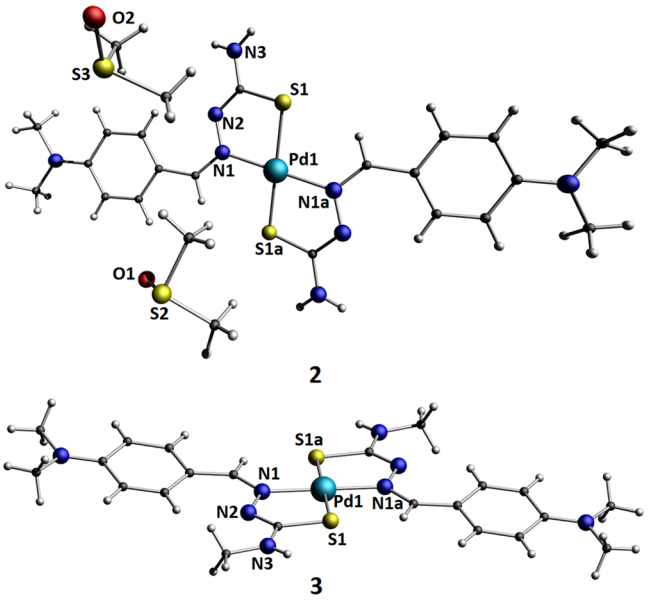

Figure 1. Representation of the X-ray structures of coordination compounds **2** and **3**. Symmetry operations: (a) $1 - x, 2 - y, -z$ (**1**); (a) $1 - x, 1 - y, 1 - z$ (**2**); (a) $-x, 1 - y, -z$ (**3**).

interactions between neighboring molecules, the shortest contact distance being of 3.597 Å (Figure 2).

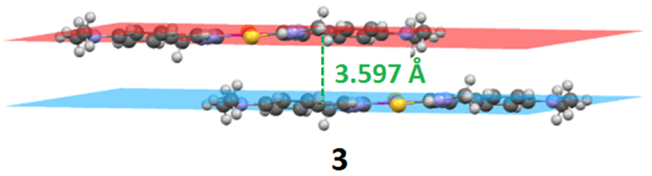

Figure 2. Representation of the crystal packing of **3** showing the stacking of molecules through $\pi-\pi$ interactions.

Stability in Solution. The stability of the coordination compounds in solution was assessed to determine the appropriate conditions to perform assays in biological media. Solution studies were thus carried out by using NMR and UV−visible spectroscopy over 24 h. Complexes **1**−**3** were dissolved in DMSO-d_6 for the NMR experiments (Figure S1), which did not reveal any spectral changes after 1 day. For the UV−vis measurements, stock solutions of **1**−**3** were prepared in DMSO, which were then used to prepare buffered aqueous solutions (Tris-HCl) of the complexes containing 5% DMSO. The UV−vis spectra displayed in Figure S2 show three intense bands in the UV region for the three complexes, ascribed to intraligand (IL) and ligand to metal charge transfer (LMCT) transitions. The absorption band around 260 nm is attributed to $\pi \rightarrow \pi^*$ (aromatic skeleton) transitions and that at about 350 nm to n $\rightarrow \pi^*$ (thioamide skeleton) transitions. The absorption band observed at ca. 400 nm is due to LMCT transitions. The compounds do not seem to be altered in solution; the same absorption bands are observed over time, and no new ones develop. However, diminutions of the absorbance intensities are noticed, which suggest that the compounds are gradually precipitating, most likely due to their poor solubility in Tris-HCl/5% DMSO. Spectroscopic studies to verify that the integrity of **1**−**3** is retained in Tris-HCl/5% DMSO were also carried out with egg-white lysozyme (HEWL), named as lysozyme thereafter. It can be pointed out here that, after 4 h, most of the compounds are in solution (i.e., significant precipitation is only observed after 24 h), hence allowing aggregation studies with Aβ(1−40) (see below).

Interaction Studies with the Model Protein Lysozyme. In a first instance, the potentially amyloidogenic protein lysozyme (hereditary lysozyme amyloidosis[38]) was used to investigate the interaction of the metal complexes with a "model protein" that is broadly employed for interaction studies with metallodrugs.[39,40] The kinetic constants corresponding to the interaction of the different compounds with lysozyme were obtained considering a pseudo-first-order reaction (see Experimental Section for details and Figure 3 and Figure S3). The values achieved (at λ = 433 nm) were compared to that of the reference compound cisplatin; k_{obs} = 1.98×10^{-4} s^{-1} was determined for cisplatin under the same experimental conditions (to those used for **1**−**3**), which matches reported values.[41]

For **1**−**3**, the kinetic data were determined from the spectra shown in Figure 3 and Figure S3. The k_{obs} values for **1** and **2** are in the range $(0.4-1) \times 10^{-4}$ s^{-1} (Table 1). Complexes **1** and **3** show about 2 times more affinity for lysozyme in comparison to **2**. The three compounds exhibit k_{obs} values 1 order of magnitude lower than that of cisplatin; **1**−**3** are certainly binding to lysozyme but less efficiently than cisplatin.

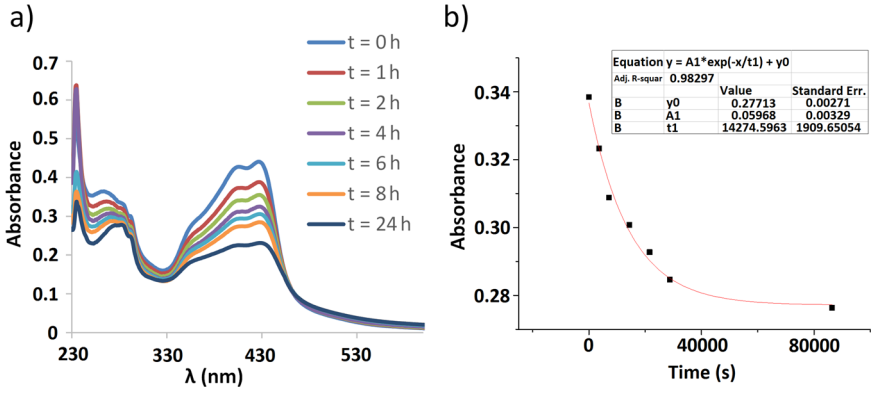

Figure 3. (a) UV−visible spectra illustrating the interaction between complex **3** (10^{-5} M; λ = 433 nm) and lysozyme (ratio 3:1) as a function of time at 37 °C and using 95% Tris-HCl (pH 7.2)/5% DMSO as a solvent. (b) Corresponding plot of the variation of the absorbance (λ = 433 nm) as a function of time. UV−visible data for complex **3** are shown in Figure S2.

https://dx.doi.org/10.1021/acs.inorgchem.0c00467
Inorg. Chem. XXXX, XXX, XXX−XXX

Table 1. k_{obs} Values Obtained for Coordination Compounds 1−3 Interacting with Lysozyme

complex	k_{obs} (10^{-5} s^{-1})
1	9.89
2	4.17
3	7.00

It has been shown that the electronic spectra of metal complexes can be modulated by their interaction with proteins; for instance, a hyperchromic effect can be observed.[42] Hence, potential changes of the UV−vis absorption properties of **1**−**3** upon interaction with lysozyme have been investigated. UV−vis spectra of **1**−**3** have therefore been recorded with and without the presence of lysozyme for 24 h. The corresponding comparative data (absorption values at λ = 433 nm) are depicted in Figure 4. In all cases, the absorptions of **1**−**3** in the presence of lysozyme are higher than those without the enzyme (Figure 4). The curves with or without lysozyme follow the same pattern, but the decrease is clearly less pronounced for the "enzyme" curves, especially for complex **3** (75 vs 37% decrease). The data thus suggest that the complexes are not degraded in solution (95% Tris-HCl/5% DMSO in the present case); hence, it appears that the complexes are poorly soluble in aqueous solutions (however, their solubility is apparently improved upon interaction with lysozyme, most likely through the formation of lysozyme/complex species). It can be pointed out that complex **3**, whose "solubilization" is sensibly improved in the presence of lysozyme, is also the biologically most efficient compound (see below).

Interaction with Aβ(1−40). The effect of the thiosemicarbazone ligands **HL**^{1}, **HL**^{2}, and **HL**^{3} and their respective palladium complexes (**1**−**3**) on the aggregation of Aβ(1−40) was subsequently evaluated *in vitro*. The aggregation of monomeric Aβ(1−40) was monitored through the changes in the fluorescence intensity of thioflavin T (ThT; specific amyloid dye) upon incubation with each compound in phosphate-buffered saline (PBS). ThT is routinely used to quantify the formation of amyloid fibrils (other probes have been regularly described[43−46]); ThT rapidly interacts with amyloid fibrils in a specific manner, resulting in an increase in its fluorescence emission at 490 nm, on excitation at 440 nm.[45−47]

The kinetic curve for the aggregation of a 25 μM solution of Aβ(1−40) monomers (**CTR**; black dots in Figure 5) shows the typical sigmoidal shape, with a lag phase (nucleation) of about 50 min, followed by a fast fibril elongation phase, which reaches a plateau after 80 min.

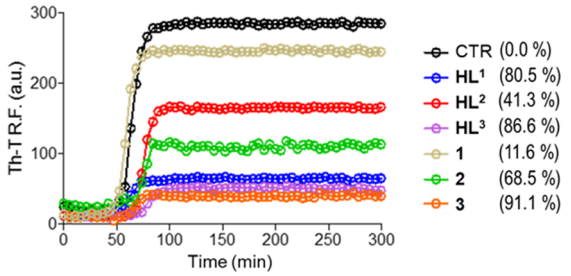

Figure 5. Time-resolved measurements of the aggregation of Aβ(1−40) through the emission of ThT at 490 nm (λ_{exc} = 440 nm) for free Aβ(1−40) (**CTR**) and Aβ(1−40) incubated with the ligands **HL**^{1}−**HL**^{3} and their metal complexes **1**−**3**. Conditions: [Aβ(1−40)] = 25 μM; [compound] = 1 μM. The respective antiaggregation efficiencies (in percent) of the compounds are given in parentheses (comparison with the control **CTR**).

In the presence of 1 μM of the different compounds (viz. **HL**^{1}−**HL**^{3}, **1**−**3**), the corresponding inhibitory activities against Aβ(1−40) fibrillation were determined over 5 h. It should be noted herein that compound **1** did not completely dissolve in PBS containing 10% DMSO. Nevertheless, for consistency, it was tested under the same conditions as for **2** and **3**, namely using 5% DMSO; thus, the data achieved with **1** should be considered cautiously. The results obtained revealed

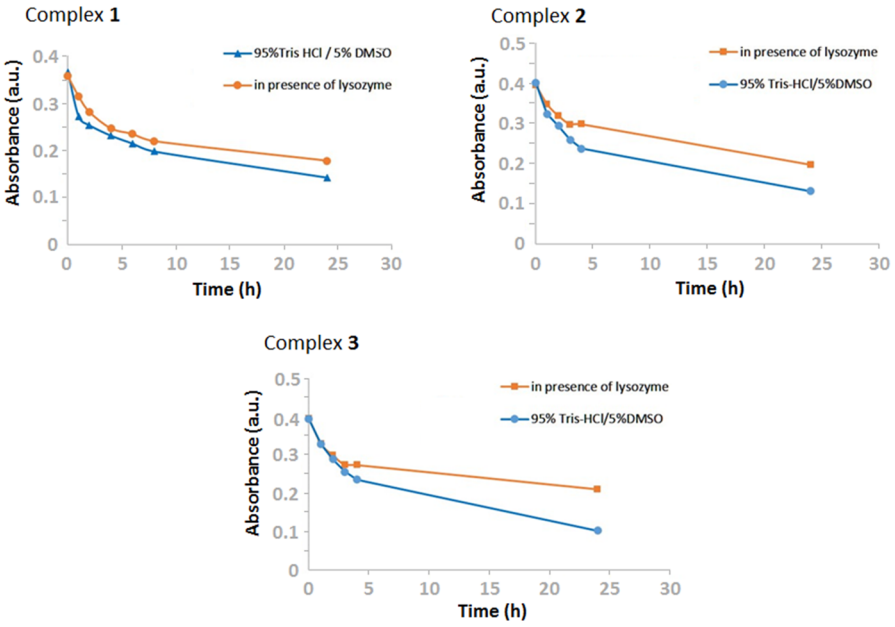

Figure 4. Time-dependent UV−visible data for complexes **1**−**3** (10^{-5} M; λ = 433 nm) in the absence and presence of lysozyme (ratio 3:1). The spectra were recorded at 37 °C using 95% Tris-HCl (pH 7.2)/5% DMSO as solvent.

https://dx.doi.org/10.1021/acs.inorgchem.0c00467
Inorg. Chem. XXXX, XXX, XXX−XXX

Table 2. Rate Constants (k_n and k_e)[a] and Fitting Time Parameters (t_0, $t_{1/2}$, and t_1)[b] and Inhibition Percentages for Free Ligands HL^1–HL^3 and Complexes 1–3 on the Aggregation of Aβ(1–40)[c]

	CTR	HL^1	HL^2	HL^3
k_n (min^{-1})	1.24×10^{-7}	2.64×10^{-7}	1.09×10^{-10}	4.06×10^{-8}
k_e (M^{-1} min^{-1})	8864	8676	11444	7684
t_0 (min)	54.3	51.6	66.7	70.7
$t_{1/2}$ (min)	65.2	62.7	76.1	79.7
t_1 (min)	76.1	73.8	85.4	88.8
inhibition (%)	0	80.5	41.3	86.6
	1		**2**	**3**
k_n (min^{-1})	8.05×10^{-8}		5.06×10^{-11}	2.45×10^{-11}
k_e (M^{-1} min^{-1})	10192		12036	13764
t_0 (min)	50.1		66.3	60.1
$t_{1/2}$ (min)	58.6		75.0	67.9
t_1 (min)	67.1		83.7	75.8
inhibition (%)	11.6		68.5	91.1

[a] k_n = nucleation rate constant; k_e = elongation rate constant (see Scheme S1). [b] t_0 = lag time; $t_{1/2}$ = time corresponding to the aggregation of 50% of the protein; t_1 = end time (plateau). [Aβ(1–40)] = 25 μM. [c] **CTR** corresponds to the fibrillation of free Aβ.

that the six new molecules could reduce Aβ(1–40) fibrillogenesis (in comparison with free Aβ; Figure 5), the final inhibition percentages ranging from 11% for **1** to 91% for **3** (Table 2). Except for partially soluble **1**, metal coordination of the thiosemicarbazones improves the antiaggregation properties; indeed, **2** and **3** show higher antiaggregation activities (68 and 91%, respectively) than the corresponding free ligands HL^2 and HL^3 (41 and 87%, respectively; Figure 5 and Table 2). In addition, HL^1, HL^3, **2**, and **3** display inhibition percentage values of higher than 50%, which correspond to remarkable IC_{50} values below 1 μM. Actually, such inhibitory data are indicative of potent antiamyloid properties since they are in the range (or even below the range) found for known polyphenolic inhibitors such as epicatechin (whose IC_{50} amounts to 2.8 μM).[48] It can also be pointed out that although ligands HL^1–HL^3 are structurally similar, they exhibit different antiaggregation properties; in particular, HL^2 is 2 times less efficient than HL^1 and HL^3. This disparity may arise from the fact that HL^2 is the sole ligand that contains an $-NH_2$ group; thus, HL^2 has three potential H-bond donors, HL^1 only one (from the hydrazine unit), and HL^3 two (see Scheme 1). Moreover, the $-NMe_2$ group of HL^1 can only act as an H-bond acceptor. It thus appears that the hydrogen-bonding properties as well as the hydrophilic character of these molecules may represent important features regarding the interaction with the protein.

The notable antiaggregation activities for all compounds (except **1**, probably as the result of its poor solubility) suggest that the scaffold of the thiosemicarbazone moieties is an important feature with regard to the observed behaviors; the flat conjugated ligands most likely interact with Aβ(1–40) through H-bonding and/or π–π interactions, as reported for other TSCN compounds (see above),[22] delaying the formation of β sheets (i.e., the fibrils).[48]

The antiaggregating activity of the compounds was further investigated by determining different kinetic parameters that allowed an assessment of their effect on the various stages of the Aβ fibrillation process (Scheme S1). The main phases of the aggregation are nucleation, characterized by the constant k_n, and elongation, described by the constant k_e (Scheme S1). This evaluation considers the amyloid aggregation as a nucleation–elongation process,[49] which can be mathematically described as an autocatalytic polymerization (see the Experimental Section for details).[50] In addition, the lag time t_0, the time for the formation of the first amyloid-like species (viz. the first nuclei), $t_{1/2}$, the time required to aggregate half of the protein to its amyloid conformation, and the end time t_1, corresponding to the completion of the fibrillation process, were determined for each compound (Scheme S1 and Table 2). All of the data obtained from the corresponding aggregation curves depicted in Figure 5 are given in Table 2.

As evidenced in Figure 5 and in Table 2, in all cases, the initiation of Aβ aggregation is not significantly delayed by the presence of the different compounds; indeed, the lag time, i.e. t_0 (see Scheme S1), for free Aβ(1–40) (**CTR**) is around 54 min, while the maximum delay observed is ca. 71 min with HL^3 (Table 2). It can be pointed out that the t_0 values are comparable for the TSCN ligands and the corresponding complexes (Table 2); only HL^3 somewhat delays the aggregation in comparison with **3** (71 vs 60 min). It can be noticed that, except for HL^1, the compounds retard the nucleation (i.e., the phase during which oligomers are generated), **2** and **3** being the most effective compounds (see k_n values in Table 2). The elongation phase, namely the phase that results in fibrils, is also affected by the presence of most of the compounds; HL^1 and HL^3 do not alter this phase, as reflected by their elongation constants, namely k_e, which are similar to that of the control (Table 2). HL^2 and **1**–**3** appear to accelerate the elongation of fibrils, with k_e values ranging from 10192 (complex **1**) to 13764 min^{-1} (compound **3**); these values should be compared with that of nontreated Aβ(1–40), namely 8864 min^{-1} (Table 2). It thus appears that, if some nuclei are generated, then these compounds facilitate their fibrilliation. However, it should be stressed that all compounds give rise to the generation of fewer amounts of fibrils at t_1 (namely, at the final plateau; see Figure 5) with percentages of inhibition ranging from 12 to 91% (Table 2); thus, the interaction of the compounds with Aβ(1–40) seems to generate stable monomeric/oligomeric species that can not fibrillate. The effiency of the different compounds follows the trend **3** > HL^3 > HL^1 > **2** ≫ HL^2 ≫ **1**. It can be noticed that coordination of palladium to the ligands results in an improvement of the inhibition properties, except for **1** (which is much less efficient than HL^1); this disparity may be explained by the poor solubility of **1** in the (biological) solvent medium used for these experiments.

https://dx.doi.org/10.1021/acs.inorgchem.0c00467
Inorg. Chem. XXXX, XXX, XXX–XXX

***In Cellulo* assays with Aβ(1−42) in Bacterial Inclusion Bodies.** The inhibition efficacies of the TSCN derivatives were then evaluated *in cellulo* with *Escherichia coli* cells expressing Aβ(1−42). After overnight incubation of the compounds with bacteria cultures, the aggregation of Aβ(1−42) was checked using Thioflavin S (ThS) and compared with that of bacteria cultured under the same conditions, but without added compound, to determine the respective inhibition percentages (Table 3). Under the conditions used (viz. final [complex] = 0.2 μM; see the Experimental Section), all of the compounds tested were not toxic to the bacteria. The results achieved show that the metal complexes **1**−**3** are much more efficient than the free ligands HL^1−HL^3. For instance, the inhibition percentage is 4.7% for HL^3 and 37.2% for **3**. In general, the coordination compounds are 7−12 times more efficient than the free TSCNs, following the trend **3** > **2** ≫ **1** > HL^3 > HL^2 ≫ HL^1. It is important to note that while the free ligands show significant inhibition properties *in vitro*, they are almost inactive *in cellulo*. For example, the inhibition percentage is 86.6% for HL^3 *in vitro* (Table 2) while it is only 4.7% *in cellulo* (Table 3); HL^3 is 18 times less efficient with bacteria. Such a drastic decrease in inhibition abilities may arise from difficulties for the TSCNs to cross the bacterial membranes, hence reducing the concentration of the effective compound inside the cells; more (biological) studies are required, however, to verify this hypothesis. In summary, the *in cellulo* results are important for two main reasons. (i) Going from *in vitro* conditions (with an isolated protein) to living cells considerably modifies the behavior of an "active compound"; thus, the use of bacteria is certainly a valuable and simple tool that may be implemented on a more regular basis, in association with *in vitro* studies. (ii) Coordination of palladium to the TSCN ligands clearly improves the *in cellulo* inhibitory activities, hence illustrating the (beneficial) role of the metal.

Table 3. Inhibition Percentages for Ligands HL^1−HL^3 and Palladium Complexes 1−3 ([Compound] = 20 μM) in Bacterial Cells Overexpressing Aβ(1−42) Monitored by ThS Staining[a]

compound	Aβ(1−42) inhibition (%)
control[b]	0.0 (1.6)
HL^1	0.8 (3.1)
HL^2	3.2 (2.0)
HL^3	4.7 (2.0)
1	9.3 (3.5)
2	22.5 (2.3)
3	37.2 (2.9)

[a]The corresponding SEM values are given in parentheses. [b]Aβ(1−42) without compound added.

CONCLUSIONS

Thiosemicarbazone derivatives have shown great promise for medicinal applications, especially in the area of anticancer agents. In the field of AD, a few studies have been reported, which revealed great potential for thiosemicarbazone-based compounds. Metal-free TSCNs have been used as efficient metal chelators: for instance to capture copper(II) ions (and potentially lessen the oxidative stress associated with AD)[28] or to inhibit Aβ aggregation.[22] With regard to metal TSCN complexes, a few compounds have been described that exhibit interesting inhibitory properties.[26,27] Their use as effective delivery vehicles for radioactive ^{64}Cu ions was reported as well, and it has been shown that Cu-TSCN complexes can cross the blood−brain barrier.[51]

In the study reported herein, we have prepared a series of TSCN ligands with the objective of comparing their inhibitory abilities against Aβ aggregation with those of their palladium(II) complexes. The data obtained show that TSCN-based molecules are indeed efficient antiaggregation agents that may therefore be considered in research aimed at developing potential anti-AD drugs. Moreover, *in cellulo* experiments with *E. coli* expressing Aβ(1−42) revealed that the palladium(II) complexes were notably more efficient inhibitors than the free TSCN ligands, illustrating the valuable effect of metal coordination and encouraging the common use of bacterial inclusion bodies as an additional experiment to accompany *in vitro* studies.

EXPERIMENTAL SECTION

Materials and Methods. Solvents and reagents were commercially available and were used as received. ^1H NMR and ^{13}C NMR experiments were performed in DMSO-d_6 using a Bruker AMX-300 (300 MHz) spectrometer at room temperature (25 °C). Elemental analyses were performed on a PerkinElmer 2400 Series II microanalyzer. Fast atom bombardment (FAB) mass spectra (MS) were recorded on a VG AutoSpec spectrometer. Infrared spectra (IR) were obtained with a PerkinElmer Model 283 spectrophotometer equipped with an ATR accessory (Miracle Single Reflection Horizontal). UV−visible spectra were recorded with a Thermo Fisher Scientific Evolution 260 Bio spectrophotometer.

Synthesis of the Compounds. *Thiosemicarbazones HL^1−HL^3.* The thiosemicarbazone ligands were prepared by following a general procedure in which a methanolic solution (10 mL) of the corresponding thiosemicarbazide (2 mmol) was added dropwise to a methanolic solution (10 mL) of 4-(dimethylamino)benzaldehyde (0.300 g, 2 mmol). The reaction mixture was refluxed with constant stirring for 6 h. Next, the mixture was cooled to ambient temperature and the solid that formed was filtered off, washed with cold methanol and diethyl ether, and dried under reduced pressure.

4-(Dimethylamino)benzaldehyde 4,4-Dimethylthiosemicarbazone (HL^1). Green solid. Yield: 92%. Anal. Calcd for $C_{12}H_{18}N_4S$: C, 57.6; H 7.2; N 22.4; S, 12.8. Found: C, 57.5; H, 7.10; N, 22.4; S, 12.6. MS (ESI) *m*/*z*: 251.13 $[M + H]^+$. ^1H NMR (300 MHz; DMSO-d_6; δ (ppm)): 2.95 (s, 6H, H_1); 3.26 (s, 6H, $H_{8/9}$); 6.75 (d, 2H, $H_{3/3'}$); 7.46 (d, 2H, $H_{4/4'}$); 8.04 (s, 1H, H_6); 10.6 (s, 1H, NH). ^{13}C NMR (300 MHz; DMSO-d_6; δ (ppm)): 40.4 (C_1); 42.1 ($C_{8/9}$); 111.8 ($C_{3/3'}$); 121.8 (C_5); 128.0 ($C_{4/4'}$); 144.8 (C_6); 151.2 (C_2); 180.1 (C_7). IR (ν; cm^{-1}): 3286 (NH); 1612 (C═N); 807 (C═S). See Scheme 1 for atom numbering.

4-(Dimethylamino)benzaldehyde Thiosemicarbazone (HL^2). Pale yellow solid. Yield: 89%. Anal. Calcd for $C_{10}H_{14}N_4S$: C, 54.0; H 6.3; N, 25.2; S, 14.4. Found: C, 53.6; H, 6.2; N, 25.2; S, 13.9. MS (ESI) *m*/*z*: 223.10 $[M + H]^+$. ^1H NMR (300 MHz; DMSO-d_6; δ (ppm)): 2.95 (s, 6H, H_1); 6.71 (d, 2H, $H_{3/3'}$); 7.55 (d, 2H, $H_{4/4'}$); 7.75 (s, 1H, $H_{8/9}$); 7.92 (s, 1H, H_6); 8.00 (s, 1H, $H_{8/9}$); 11.10 (s, 1H, NH). ^{13}C NMR (300 MHz; DMSO-d_6; δ (ppm)): 40.0 (C_1); 111.6 ($C_{3/3'}$); 121.8 (C_5); 128.6 ($C_{4/4'}$); 143.3 (C_6); 151.3 (C_2); 180.0 (C_7). IR (ν; cm^{-1}): 3414, 3229 (NH); 1614 (C═N); 808 (C═S). See Scheme 1 for atom numbering.

4-(Dimethylamino)benzaldehyde 4-Methylthiosemicarbazone (HL^3). Pale yellow solid. Yield: 90%. Anal. Calcd for $C_{11}H_{16}N_4S$: C, 55.9; H, 6.82; N, 23.7; S, 13.6. Found: C, 55.8; H 6.70; N, 22.9; S, 13.4. MS (ESI) *m*/*z*: 237.12 $[M + H]^+$. ^1H NMR (300 MHz; DMSO-d_6; δ (ppm)): 2.96 (s, 6H, H_1); 3.00 (s, 3H, H_9); 6.72 (d, 2H, $H_{3/3'}$); 7.56 (d, 2H, $H_{4/4'}$); 7.94 (s, 1H, H_6); 8.26 (s, 1H, H_8); 11.20 (s, 1H, NH). ^{13}C NMR (300 MHz; DMSO-d_6; δ (ppm)): 30.4 (C_9); 41.3 (C_1); 111.4 ($C_{3/3'}$); 121.3 (C_5); 128.2 ($C_{4/4'}$), 142.5(C_6); 151.0 (C_2); 179.8 (C_7). IR (ν; cm^{-1}): 3328, 3142 (NH); 1612 (C═N); 812 (C═S). See Scheme 1 for atom numbering.

https://dx.doi.org/10.1021/acs.inorgchem.0c00467
Inorg. Chem. XXXX, XXX, XXX−XXX

Coordination Compounds ***1*–*3***: *Pd(**L**^{1})$_2$* ***(1)***, *Pd(**L**^{2})$_2$* ***(2)***, *and Pd(**L**^{3})$_2$* ***(3)***. The palladium(II) complexes were obtained by reaction of a methanolic suspension of the corresponding ligand (0.4 mmol) with a methanolic solution of lithium tetrachloridopalladate(II), prepared *in situ* from palladium chloride(II) (0.2 mmol) and lithium chloride (0.8 mmol). The reaction mixture was stirred for 24 h at room temperature, and the solid obtained was subsequently filtered off and washed with water, methanol, and diethyl ether. The isolated solid was finally dried under reduced pressure.

*Pd(**L**^{1})$_2$* ***(1)***. Brown solid; Yield: 68%. Anal. Calcd for $PdC_{24}H_{34}N_8S_2$: C, 47.6; H, 5.66; N, 18.5; S, 10.6. Found: C, 46.4; H, 6.56; N, 18.3; S, 10.5. MS (ESI) *m*/*z*: 605.2 $[M + H]^+$. ^{1}H NMR (300 MHz; DMSO-d_6; δ (ppm)): 3.01 (s, 12H, H_1); 3.19 (s, 12H, $H_{8/9}$); 6.73 (d, 4H, $H_{3/3'}$); 7.22 (s, 2H, H_6); 7.91 (d, 4H, $H_{4/4'}$). IR (ν; cm^{-1}): 3276 (NH); 1584 (C═N−N═C); 711 (C−S). See Scheme 1 for atom numbering.

*Pd(**L**^{2})$_2$* ***(2)***. Brown solid; Yield: 70%. Anal. Calcd for $PdC_{20}H_{26}N_8S_2{\cdot}5H_2O$: C, 37.6; H, 5.68; N, 17.5; S, 10.0. Found: C, 37.3; H, 4.64; N, 17.3; S, 10.3. MS (ESI) *m*/*z*: 551.10 $[M + H]^+$. ^{1}H NMR (300 MHz; DMSO-d_6; δ (ppm)): 3.02 (s, 12H, H_1); 6.67 (d, 4H, $H_{3/3'}$); 6.95 (s, 4H, $H_{8/9}$); 7.22 (s, 2H, H_6); 8.00 (d, 4H, $H_{4/4'}$). ^{13}C NMR (300 MHz; DMSO-d_6; δ (ppm)): 48.6 (C_1); 110.9 ($C_{3/3'}$); 118.5 (C_5); 134.9 ($C_{4/4'}$); 144.8 (C_6); 151.2 (C_2); 180.1 (C_7). IR (ν; cm^{-1}): 3276 (NH); 1600 (C═N−N═C); 789 (C−S). Single crystals suitable for X-ray diffraction analysis were obtained by recrystallization from DMSO. See Scheme 1 for atom numbering.

*Pd(**L**^{3})$_2$* ***(3)***. Brown solid; Yield: 69%. Anal. Calcd for $PdC_{22}H_{32}N_8S_2{\cdot}H_2O$: C, 44.4; H, 5.4; N, 18.8; S, 11.0. Found: C, 44.0; H, 5.1; N, 18.5; S, 10.4. MS (FAB) *m*/*z*: 576.11 $[M + H]^+$. ^{1}H NMR (300 MHz; DMSO-d_6; δ (ppm)): 2.80 (s, 6H, H_9); 3.01 (s, 12H, H_1); 6.70 (d, 4H, $H_{3/3'}$); 7.16 (s, 2H, H_6); 7.93 (d, 4H, $H_{4/4'}$). ^{13}C NMR (300 MHz; DMSO-d_6; δ (ppm)): 32.3 (C_9); 40.0 (C_1); 111.0 ($C_{3/3'}$); 119.9 (C_5); 128.5 ($C_{4/4'}$); 134.1 (C_6); 134.4(C_2); 151.2 (C_7). IR (ν; cm^{-1}): 3409 (NH); 1600 (C═N−N═C); 754 (C−S). Single crystals suitable for X-ray diffraction analysis were obtained by recrystallization from DMSO. See Scheme 1 for atom numbering.

Crystallography. Data were collected on a Bruker Kappa Apex II diffractometer. Crystallographic and refinement parameters are summarized in Table S1. The software package SHELXTL was used for space group determination, structure solution, and refinement.[52] The structures were solved by direct methods, completed with difference Fourier syntheses, and refined with anisotropic displacement parameters.

All details can be found in CCDC 1884751 (**2**) and 1884752 (**3**), which contain the supplementary crystallographic data for this paper. These data can be obtained free of charge from The Cambridge Crystallographic Data Center via https://summary.ccdc.cam.ac.uk/structure-summary-form.

Spectrophotometric Studies. The solution stabilities of complexes **1**−**3** were evaluated by recording their UV−vis spectra for 24 h at 37 °C and a concentration of 10^{-5} M. Time-dependent UV−vis spectra of the complexes in the presence of a biomolecule, namely lysozyme, have been registered as well.

Interaction with Lysozyme Followed by UV−vis Spectroscopy. The interaction of the metal complexes with lysozyme (egg white lysozyme; HEWL) was investigated using a 10^{-5} M solution of the protein. Lysozyme is a widely used model protein for studying the binding of potential metallodrugs; lysozyme is also a model amyloid-forming protein. The integrity of the enzyme was checked in each experiment, with a comparison of fresh and incubated samples. UV−vis spectra were recorded before and after incubation with the different complexes (dissolved in 95% Tris-HCl/5% DMSO) for 24 h at 37 °C. A metal to protein ratio of 3:1 was used for these studies. The experimental time-dependent profiles of the spectra were analyzed as pseudo-first-order reactions by plotting the variation of the absorbance as a function of time. The absorption profiles are shown in Figure 3a (**3**) and Figure S3 (**1** and **2**).

***In Vitro* studies of Aβ(1−40) Aggregation.** *Preparation of Aggregate-Free Amyloid-β.* Aβ(1−40) (5 mg) was solubilized in 1,1,1,3,3,3-hexafluoro-2-propanol (HFIP; 1 mL) with vigorous shaking at room temperature for 1 h. The resulting solution was sonicated for 30 min and subsequently shaken at room temperature for an additional 1 h. The solution was then maintained at 4 °C for 30 min to avoid solvent evaporation during the collection of aliquots. HFIP was evaporated under a gentle stream of nitrogen, and the aliquots of soluble Aβ(1−40) were stored at −20 °C.

Amyloid-β Aggregation Studies. Aβ(1−40) aliquots were resuspended in 30 μL of DMSO, and the monomers were solubilized through sonication for 10 min. PBS buffer (pH 7.4), 500 μM thioflavin T (ThT), and 0.2 mM stock solution (in DMSO) of the compound to be tested were added to the Aβ(1−40) sample (final concentration of compound: 1 μM). PBS buffer (pH 7.4) was then added to obtain final solutions of 25 μM Aβ(1−40) and 34 μM ThT, containing 4.4% (v/v) DMSO. Control experiments with nontreated protein samples contained the same amount of DMSO as in the samples containing the compounds investigated. For the kinetic assays, the samples were placed in a 96-well plate at 37 °C and stirred at 700 rpm with double-orbital mode. The course of the aggregation was followed by measuring ThT fluorescence using a FLUOstar OMEGA plate reader (BMG Labtech GmbH), with excitation and emission filters of 440 and 490 nm, respectively.

Aggregation Assay Analysis. The amyloid aggregation can be studied as an autocatalytic reaction using eq 1

$$f = \frac{\rho\{\exp[(1+\rho)^{kt}] - 1\}}{1 + \rho\exp[(1+\rho)^{kt}]} \quad (1)$$

where f is the fraction of fibrillary Aβ and the rate constant k includes the kinetic contributions arising from the formation of the nucleus from monomeric Aβ and the elongation of the fibril, which are described by the rate constants k_n and k_e, respectively. ρ is a dimensionless parameter that describes the ratio of k_n to k. Equation 1 is obtained under the boundary conditions of $t = 0$ and $f = 0$, where $k = k_e a$ (a is the protein concentration). By nonlinear regression of f against t, values for ρ and k were obtained, and from them the rate constants k_e (elongation constant) and k_n (nucleation constant) were determined.[50] The extrapolation of the linear portion of the sigmoid curve to the abscissa ($f = 0$) and to the highest ordinate value of the fitted plot afforded two values of time, namely t_0 and t_1, which corresponded to the lag time and to the end time of the reaction, respectively. The time at which half of the protein was aggregated (i.e., when $f = 0.5$) was considered as the time of half an aggregation (viz. $t_{1/2}$).[50]

The estimation of the IC_{50} values and of the kinetic data from the autocatalytic eq 1 was carried out using GraphPad Prism (GraphPad Software, La Jolla, CA, USA).

***In Cellulo* Assays of Aβ(1−42) Aggregation.** *Escherichia coli* competent cells BL21 (DE3) were transformed with the pET28a vector from Novagen carrying the DNA sequence of Aβ(1−42). A 10 mL of M9 minimal medium containing 50 μg mL^{-1} of kanamycin was inoculated with a single colony of BL21 (DE3) bearing the plasmid to be expressed, and the bacteria were cultured overnight at 37 °C. For Aβ(1−42) expression, 200 μL of the culture (incubated overnight) was transferred into 1.5 mL microcentrifuge tubes with 790 μL of fresh M9 minimal medium, giving final concentrations of 50 μg mL^{-1} of kanamycin and 25 μM of thioflavin S (ThS); 10 μL of 100 mM isopropyl 1-thio-β-D-galactopyranoside (IPTG) was added or not, for induced and noninduced cultures, respectively. Then, 10 μL of each TSCN-based compound (different ligands and Pd complexes) with the required concentration (20 μM) was added, giving a final complex concentration of 0.2 μM. The samples were grown overnight at 37 °C and at 300 rpm, using an incubator with orbital shaking. As a control of maximal amyloid formation, samples for which the 10 μL of compound solution was replaced by 10 μL of buffer were analyzed as well. Aβ(1−42) aggregation was followed by fluorescence spectroscopy, using thioflavin S (ThS). Variations in ThS fluorescence intensities due to potential differences in bacterial growth between samples (the growth of induced bacteria may slightly be lower than

https://dx.doi.org/10.1021/acs.inorgchem.0c00467
Inorg. Chem. XXXX, XXX, XXX−XXX

that of noninduced bacteria), were corrected by tracking the absorbance at 405 nm.

■ ASSOCIATED CONTENT

Supporting Information

The Supporting Information is available free of charge at https://pubs.acs.org/doi/10.1021/acs.inorgchem.0c00467.

> Crystallographic data for compounds **2** and **3**, time-dependent NMR spectra of **1**−**3** in DMSO-d_6, time-dependent UV−vis spectra for **1**−**3** in Tris-HCl/5% DMSO, UV−vis spectra for **1**−**3** interacting with lysozyme, NMR and mass spectra for compounds **HL1**−**HL3**, and schematic representation of Aβ fibrillation (PDF)

Accession Codes

CCDC 1884751−1884752 contain the supplementary crystallographic data for this paper. These data can be obtained free of charge via www.ccdc.cam.ac.uk/data_request/cif, or by emailing data_request@ccdc.cam.ac.uk, or by contacting The Cambridge Crystallographic Data Centre, 12 Union Road, Cambridge CB2 1EZ, UK; fax: +44 1223 336033.

■ AUTHOR INFORMATION

Corresponding Authors

Adoración G. Quiroga − *Institute for Advanced Research in Chemical Sciences (IAdChem) and Department of Inorganic Chemistry (M-07), School of Sciences, Universidad Autónoma de Madrid, Madrid 28049, Spain;* orcid.org/0000-0002-9261-9542; Email: adoracion.gomez@uam.es

Patrick Gamez − *nanoBIC, Departament de Química Inorgànica i Orgànica, Facultat de Química and Institute of Nanoscience and Nanotechnology (IN2UB), Universitat de Barcelona, 08028 Barcelona, Spain; Catalan Institution for Research and Advanced Studies, 08010 Barcelona, Spain;* orcid.org/0000-0003-2602-9525; Phone: +34 934 021274; Email: patrick.gamez@qi.ub.es

Authors

Ana I. Matesanz − *Department of Inorganic Chemistry (M-07), School of Sciences, Universidad Autónoma de Madrid, 28049 Madrid, Spain;* orcid.org/0000-0002-6113-0656

Ana B. Caballero − *nanoBIC, Departament de Química Inorgànica i Orgànica, Facultat de Química and Institute of Nanoscience and Nanotechnology (IN2UB), Universitat de Barcelona, 08028 Barcelona, Spain;* orcid.org/0000-0001-9294-9085

Carmen Lorenzo − *Department of Inorganic Chemistry (M-07), School of Sciences, Universidad Autónoma de Madrid, 28049 Madrid, Spain*

Alba Espargaró − *Departament de Fisicoquímica, Facultat de Farmàcia i Ciències de l'Alimentació and Institute of Nanoscience and Nanotechnology (IN2UB), Universitat de Barcelona, 08028 Barcelona, Spain*

Raimon Sabaté − *Departament de Fisicoquímica, Facultat de Farmàcia i Ciències de l'Alimentació and Institute of Nanoscience and Nanotechnology (IN2UB), Universitat de Barcelona, 08028 Barcelona, Spain;* orcid.org/0000-0003-3894-2362

Complete contact information is available at: https://pubs.acs.org/10.1021/acs.inorgchem.0c00467

Author Contributions

The manuscript was written through contributions of all authors. All authors have given approval to the final version of the manuscript.

Notes

The authors declare no competing financial interest.

■ ACKNOWLEDGMENTS

Financial support from the Spanish Ministerio de Ciencia Innovación, y Universidades (Projects CTQ2015-70371, CTQ2015-68779-R and CTQ2017-88446-R AEI/FEDER, UE and RED2018-102471-T) is kindly acknowledged. P.G. acknowledges the Institució Catalana de Recerca i Estudis Avançats (ICREA).

■ REFERENCES

(1) Masters, C. L.; Cappai, R.; Barnham, K. J.; Villemagne, V. L. Molecular mechanisms for Alzheimer's disease: implications for neuroimaging and therapeutics. *J. Neurochem.* **2006**, *97* (6), 1700−1725.

(2) World Health Organization Dementia; http://www.who.int/news-room/fact-sheets/detail/dementia (November 28, 2018).

(3) Wang, J.; Gu, B. J.; Masters, C. L.; Wang, Y. J. A systemic view of Alzheimer disease - insights from amyloid-beta metabolism beyond the brain. *Nat. Rev. Neurol.* **2017**, *13* (10), 612−623.

(4) Duce, J. A.; Bush, A. I.; Adlard, P. A. Role of amyloid-b−metal interactions in Alzheimer's disease. *Future Neurol.* **2011**, *6* (5), 641−659.

(5) Masters, C. L.; Simms, G.; Weinman, N. A.; Multhaup, G.; McDonald, B. L.; Beyreuther, K. Amyloid plaque core protein in Alzheimer disease and Down syndrome. *Proc. Natl. Acad. Sci. U. S. A.* **1985**, *82* (12), 4245−4249.

(6) Masters, C. L.; Selkoe, D. J. Biochemistry of Amyloid beta-Protein and Amyloid Deposits in Alzheimer Disease. *Cold Spring Harbor Perspect. Med.* **2012**, *2* (6), a006262.

(7) Ayton, S.; Fazlollahi, A.; Bourgeat, P.; Raniga, P.; Ng, A.; Lim, Y. Y.; Diouf, I.; Farquharson, S.; Fripp, J.; Ames, D.; Doecke, J.; Desmond, P.; Ordidge, R.; Masters, C. L.; Rowe, C. C.; Maruff, P.; Villemagne, V. L.; Salvado, O.; Bush, A. I. Cerebral quantitative susceptibility mapping predicts amyloid-beta-related cognitive decline. *Brain* **2017**, *140*, 2112−2119.

(8) Bandyopadhyay, S.; Huang, X. D.; Lahiri, D. K.; Rogers, J. T. Novel drug targets based on metallobiology of Alzheimer's disease. *Expert Opin. Ther. Targets* **2010**, *14* (11), 1177−1197.

(9) Peters, D. G.; Connor, J. R.; Meadowcroft, M. D. The relationship between iron dyshomeostasis and amyloidogenesis in Alzheimer's disease: Two sides of the same coin. *Neurobiol. Dis.* **2015**, *81*, 49−65.

(10) Cheignon, C.; Tomas, M.; Bonnefont-Rousselot, D.; Faller, P.; Hureau, C.; Collin, F. Oxidative stress and the amyloid beta peptide in Alzheimer's disease. *Redox Biol.* **2018**, *14*, 450−464.

(11) Moorthy, N.; Cerqueira, N.; Ramos, M. J.; Fernandes, P. A. Aryl- and Heteroaryl-Thiosemicarbazone Derivatives and Their Metal Complexes: A Pharmacological Template. *Recent Pat. Anti-Cancer Drug Discovery* **2013**, *8* (2), 168−182.

(12) Lukmantara, A. Y.; Kalinowski, D. S.; Kumar, N.; Richardson, D. R. Synthesis and biological evaluation of 2-benzoylpyridine thiosemicarbazones in a dimeric system: Structure-activity relationship studies on their anti-proliferative and iron chelation efficacy. *J. Inorg. Biochem.* **2014**, *141*, 43−54.

(13) Chellan, P.; Stringer, T.; Shokar, A.; Dornbush, P. J.; Vazquez-Anaya, G.; Land, K. M.; Chibale, K.; Smith, G. S. Synthesis and in vitro evaluation of palladium(II) salicylaldiminato thiosemicarbazone complexes against Trichomonas vaginalis. *J. Inorg. Biochem.* **2011**, *105* (12), 1562−1568.

(14) Indoria, S.; Lobana, T. S.; Sood, H.; Arora, D. S.; Hundal, G.; Jasinski, J. P. Synthesis, spectroscopy, structures and antimicrobial

activity of mixed-ligand zinc(II) complexes of 5-nitro-salicylaldehyde thiosemicarbazones. *New J. Chem.* **2016**, *40* (4), 3642−3653.
(15) Pelosi, G.; Bisceglie, F.; Bignami, F.; Ronzi, P.; Schiavone, P.; Re, M. C.; Casoli, C.; Pilotti, E. Antiretroviral Activity of Thiosemicarbazone Metal Complexes. *J. Med. Chem.* **2010**, *53* (24), 8765−8769.
(16) Heffeter, P.; Pape, V. F. S.; Enyedy, E. A.; Keppler, B. K.; Szakacs, G.; Kowol, C. R. Anticancer Thiosemicarbazones: Chemical Properties, Interaction with Iron Metabolism, and Resistance Development. *Antioxid. Redox Signaling* **2019**, *30*, 1062.
(17) Richardson, D. R.; Sharpe, P. C.; Lovejoy, D. B.; Senaratne, D.; Kalinowski, D. S.; Islam, M.; Bernhardt, P. V. Dipyridyl thiosemicarbazone chelators with potent and selective antitumor activity form iron complexes with redox activity. *J. Med. Chem.* **2006**, *49* (22), 6510−6521.
(18) Gomes, L. M. F.; Vieira, R. P.; Jones, M. R.; Wang, M. C. P.; Dyrager, C.; Souza-Fagundes, E. M.; Da Silva, J. G.; Storr, T.; Beraldo, H. 8-Hydroxyquinoline Schiff-base compounds as antioxidants and modulators of copper-mediated A beta peptide aggregation. *J. Inorg. Biochem.* **2014**, *139*, 106−116.
(19) Pelivan, K.; Frensemeier, L.; Karst, U.; Koellensperger, G.; Bielec, B.; Hager, S.; Heffeter, P.; Keppler, B. K.; Kowol, C. R. Understanding the metabolism of the anticancer drug Triapine: electrochemical oxidation, microsomal incubation and in vivo analysis using LC-HRMS. *Analyst* **2017**, *142* (17), 3165−3176.
(20) Guo, Z. L.; Richardson, D. R.; Kalinowski, D. S.; Kovacevic, Z.; Tan-Un, K. C.; Chan, G. C. F. The novel thiosemicarbazone, di-2-pyridylketone 4-cyclohexyl-4-methyl-3-thiosemicarbazone (DpC), inhibits neuroblastoma growth in vitro and in vivo via multiple mechanisms. *J. Hematol. Oncol.* **2016**, *9*, 98.
(21) Chao, J.; Synold, T. W.; Morgan, R. J.; Kunos, C.; Longmate, J.; Lenz, H. J.; Lim, D.; Shibata, S.; Chung, V.; Stoller, R. G.; Belani, C. P.; Gandara, D. R.; McNamara, M.; Gitlitz, B. J.; Lau, D. H.; Ramalingam, S. S.; Davies, A.; Espinoza-Delgado, I.; Newman, E. M.; Yen, Y. A phase I and pharmacokinetic study of oral 3-aminopyridine-2-carboxaldehyde thiosemicarbazone (3-AP, NSC #663249) in the treatment of advanced-stage solid cancers: a California Cancer Consortium Study. *Cancer Chemother. Pharmacol.* **2012**, *69* (3), 835−843.
(22) Ranade, D. S.; Shravage, B. V.; Kumbhar, A. A.; Sonawane, U. B.; Jani, V. P.; Joshi, R. R.; Kulkarni, P. P. Thiosemicarbazone Moiety Assist in Interaction of Planar Aromatic Molecules with Amyloid Beta Peptide and Acetylcholinesterase. *ChemistrySelect* **2017**, *2* (13), 3911−3916.
(23) Ranade, D. S.; Bapat, A. M.; Ramteke, S. N.; Joshi, B. N.; Roussel, P.; Tomas, A.; Deschamps, P.; Kulkarni, P. P. Thiosemicarbazone modification of 3-acetyl coumarin inhibits A beta peptide aggregation and protect against A beta-induced cytotoxicity. *Eur. J. Med. Chem.* **2016**, *121*, 803−809.
(24) Haribabu, J.; Ranade, D. S.; Bhuvanesh, N. S. P.; Kulkarni, P. P.; Karvembu, R. Ru(II)-p-cymene Thiosemicarbazone Complexes as Inhibitors of Amyloid beta (A beta) Peptide Aggregation and A beta-Induced Cytotoxicity. *ChemistrySelect* **2017**, *2* (35), 11638−11644.
(25) Palanimuthu, D.; Poon, R.; Sahni, S.; Anjum, R.; Hibbs, D.; Lin, H. Y.; Bernhardt, P. V.; Kalinowski, D. S.; Richardson, D. R. A novel class of thiosemicarbazones show multi-functional activity for the treatment of Alzheimer's disease. *Eur. J. Med. Chem.* **2017**, *139*, 612−632.
(26) Lim, S.; Paterson, B. M.; Fodero-Tavoletti, M. T.; O'Keefe, G. J.; Cappai, R.; Barnham, K. J.; Villemagne, V. L.; Donnelly, P. S. A copper radiopharmaceutical for diagnostic imaging of Alzheimer's disease: a bis(thiosemicarbazonato)copper(II) complex that binds to amyloid-beta plaques. *Chem. Commun.* **2010**, *46* (30), 5437−5439.
(27) Donnelly, P. S.; Caragounis, A.; Du, T.; Laughton, K. M.; Volitakis, I.; Cherny, R. A.; Sharples, R. A.; Hill, A. F.; Li, Q. X.; Masters, C. L.; Barnham, K. J.; White, A. R. Selective intracellular release of copper and zinc ions from bis(thiosemicarbazonato) complexes reduces levels of Alzheimer disease amyloid-beta peptide. *J. Biol. Chem.* **2008**, *283* (8), 4568−4577.
(28) D'Acunto, C. W.; Kaplanek, R.; Gbelcova, H.; Kejik, Z.; Briza, T.; Vasina, L.; Havlik, M.; Ruml, T.; Kral, V. Metallomics for Alzheimer's disease treatment: Use of new generation of chelators combining metal-cation binding and transport properties. *Eur. Eur. J. Med. Chem.* **2018**, *150*, 140−155.
(29) Arai, T.; Araya, T.; Sasaki, D.; Taniguchi, A.; Sato, T.; Sohma, Y.; Kanai, M. Rational Design and Identification of a Non-Peptidic Aggregation Inhibitor of Amyloid-beta Based on a Pharmacophore Motif Obtained from cyclo[-Lys-Leu-Val-Phe-Phe-]. *Angew. Chem., Int. Ed.* **2014**, *53* (31), 8236−8239.
(30) Quiroga, A. G.; Ranninger, C. N. Contribution to the SAR field of metallated and coordination complexes. Studies of the palladium and platinum derivatives with selected thiosemicarbazones as antitumoral drugs. *Coord. Chem. Rev.* **2004**, *248* (1−2), 119−133.
(31) Matesanz, A. I.; Jimenez-Faraco, E.; Ruiz, M. C.; Balsa, L. M.; Navarro-Ranninger, C.; Leon, I. E.; Quiroga, A. G. Mononuclear Pd(II) and Pt(II) complexes with an alpha-N-heterocyclic thiosemicarbazone: cytotoxicity, solution behaviour and interaction versus proven models from biological media. *Inorg. Chem. Front.* **2018**, *5* (1), 73−83.
(32) Fanelli, M.; Formica, M.; Fusi, V.; Giorgi, L.; Micheloni, M.; Paoli, P. New trends in platinum and palladium complexes as antineoplastic agents. *Coord. Chem. Rev.* **2016**, *310*, 41−79.
(33) Alam, M. N.; Huq, F. Comprehensive review on tumour active palladium compounds and structure-activity relationships. *Coord. Chem. Rev.* **2016**, *316*, 36−67.
(34) Paul, P.; Datta, S.; Halder, S.; Acharyya, R.; Basuli, F.; Butcher, R. J.; Peng, S. M.; Lee, G. H.; Castineiras, A.; Drew, M. G. B.; Bhattacharya, S. Syntheses, structures and efficient catalysis for C-C coupling of some benzaldehyde thiosemicarbazone complexes of palladium. *J. Mol. Catal. A: Chem.* **2011**, *344* (1−2), 62−73.
(35) Caballero, A. B.; Espargaro, A.; Pont, C.; Busquets, M. A.; Estelrich, J.; Munoz-Torrero, D.; Gamez, P.; Sabate, R. Bacterial Inclusion Bodies for Anti-Amyloid Drug Discovery: Current and Future Screening Methods. *Curr. Protein Pept. Sci.* **2019**, *20* (6), 563−576.
(36) Purohit, S.; Koley, A. P.; Prasad, L. S.; Manoharan, P. T.; Ghosh, S. Chemistry of molybdenum with hard-soft donor ligands. 2. Molybdenum (VI), -(V), and -(IV) oxo complexes with tridentate Schiff base ligands. *Inorg. Chem.* **1989**, *28* (19), 3735−3742.
(37) Jing, X.; Yang, Y.; He, C.; Chang, Z. D.; Reek, J. N. H.; Duan, C. Y. Control of Redox Events by Dye Encapsulation Applied to Light-Driven Splitting of Hydrogen Sulfide. *Angew. Chem., Int. Ed.* **2017**, *56* (39), 11759−11763.
(38) Benyamine, A.; Bernard-Guervilly, F.; Tummino, C.; Macagno, N.; Daniel, L.; Valleix, S.; Granel, B. Hereditary lysozyme amyloidosis with sicca syndrome, digestive, arterial, and tracheobronchial involvement: case-based review. *Clin. Rheumatol.* **2017**, *36* (11), 2623−2628.
(39) Casini, A.; Mastrobuoni, G.; Temperini, C.; Gabbiani, C.; Francese, S.; Moneti, G.; Supuran, C. T.; Scozzafava, A.; Messori, L. ESI mass spectrometry and X-ray diffraction studies of adducts between anticancer platinum drugs and hen egg white lysozyme. *Chem. Commun.* **2007**, *2*, 156−158.
(40) Ferraro, G.; Marzo, T.; Infrasca, T.; Cilibrizzi, A.; Vilar, R.; Messori, L.; Merlino, A. A case of extensive protein platination: the reaction of lysozyme with a Pt(II)-terpyridine complex. *Dalton Trans.* **2018**, *47* (26), 8716−8723.
(41) Echeverri, M.; Alvarez-Valdes, A.; Navas, F.; Perles, J.; Sanchez-Perez, I.; Quiroga, A. G. Using phosphine ligands with a biological role to modulate reactivity in novel platinum complexes. *R. Soc. Open Sci.* **2018**, *5* (2), 171340.
(42) Annunziata, A.; Amoresano, A.; Cucciolito, M. E.; Esposito, R.; Ferraro, G.; Iacobucci, I.; Imbimbo, P.; Lucignano, R.; Melchiorre, M.; Monti, M.; Scognamiglio, C.; Tuzi, A.; Monti, D. M.; Merlino, A.; Ruffo, F. Pt(II) versus Pt(IV) in Carbene Glycoconjugate Antitumor Agents: Minimal Structural Variations and Great Performance Changes. *Inorg. Chem.* **2020**, *59* (6), 4002−4014.

https://dx.doi.org/10.1021/acs.inorgchem.0c00467
Inorg. Chem. XXXX, XXX, XXX−XXX

(43) Xu, M. M.; Ren, W. M.; Tang, X. C.; Hu, Y. H.; Zhang, H. Y. Advances in development of fluorescent probes for detecting amyloid-beta aggregates. *Acta Pharmacol. Sin.* **2016**, *37* (6), 719−730.
(44) Peng, C.; Wang, X. L.; Li, Y. H.; Li, H. W.; Wong, M. S. Versatile fluorescent probes for near-infrared imaging of amyloid-beta species in Alzheimer's disease mouse model. *J. Mater. Chem. B* **2019**, *7* (12), 1986−1995.
(45) Man, B. Y. W.; Chan, H. M.; Leung, C. H.; Chan, D. S. H.; Bai, L. P.; Jiang, Z. H.; Li, H. W.; Ma, D. L. Group 9 metal-based inhibitors of beta-amyloid (1−40) fibrillation as potential therapeutic agents for Alzheimer's disease. *Chem. Sci.* **2011**, *2* (5), 917−921.
(46) Baranello, R. J.; Bharani, K. L.; Padmaraju, V.; Chopra, N.; Lahiri, D. K.; Greig, N. H.; Pappolla, M. A.; Sambamurti, K. Amyloid-Beta Protein Clearance and Degradation (ABCD) Pathways and their Role in Alzheimer's Disease. *Curr. Alzheimer Res.* **2015**, *12* (1), 32−46.
(47) Xue, C.; Lin, T. Y. W.; Chang, D.; Guo, Z. F. Thioflavin T as an amyloid dye: fibril quantification, optimal concentration and effect on aggregation. *R. Soc. Open Sci.* **2017**, *4* (1), 160696. and references therein
(48) Porat, Y.; Abramowitz, A.; Gazit, E. Inhibition of amyloid fibril formation by polyphenols: Structural similarity and aromatic interactions as a common inhibition mechanism. *Chem. Biol. Drug Des.* **2006**, *67* (1), 27−37.
(49) Jarrett, J. T.; Lansbury, P. T. Seeding "one-dimensional crystallization" of amyloid: a pathogenic mechanism in Alzheimer's disease and scrapie? *Cell* **1993**, *73* (6), 1055−1058.
(50) Sabate, R.; Gallardo, M.; Estelrich, J. An autocatalytic reaction, as a model for the kinetics of the aggregation of beta-amyloid. *Biopolymers* **2003**, *71* (2), 190−195.
(51) Hayne, D. J.; Lim, S.; Donnelly, P. S. Metal complexes designed to bind to amyloid-beta for the diagnosis and treatment of Alzheimer's disease. *Chem. Soc. Rev.* **2014**, *43* (19), 6701−6715.
(52) *SHELTXTL-NT Structure Determination Package, ver. 6.12*; Bruker-Nonius AXS: Madison, WI, USA, 1997−2001.

https://dx.doi.org/10.1021/acs.inorgchem.0c00467
Inorg. Chem. XXXX, XXX, XXX−XXX